Journal of
Water & Climate Change

IWA PUBLISHING

Journal of Water and Climate Change Vol 15 No 3, 1313 doi: 10.2166/wcc.2024.595

Assessment of surface water dynamics through satellite mapping with Google Earth Engine and Sentinel-2 data in Manipur, India

Vanita Pandey, Pankaj Kumar Pandey *, Pema Tshering Lepcha and Naorem Nirmala Devi

Department of Agricultural Engineering, North Eastern Regional Institute of Science and Technology (NERIST), Nirjuli, Itanagar, Arunachal Pradesh, India
*Corresponding author. E-mail: pandeypk@gmail.com; pkp@nerist.ac.in

PKP, 0000-0002-5936-3565

ABSTRACT

Accurate surface water mapping is crucial for watershed planning and safeguarding regional water resources. The study aimed to extract the extent of seasonal surface water, focusing on selected districts of Manipur, northeast India from 2016 to 2021, utilizing Sentinel-2 data in the Google Earth Engine (GEE) platform. Employing multiple indices and the Random Forest classifier, the methodology addressed challenges such as cloud and shadow interference, particularly in high-altitude regions. Results revealed Bishnupur had the maximum surface water extent (124 km^2) and Tengnoupal had the minimum (0.24 km^2) during the study period. A notable 6% gain in Bishnupur surface water was observed from pre- to post-monsoon in 2016, while changes in other districts were negligible. Conversely, a maximum loss of 7% occurred in Bishnupur during pre-monsoon from 2016 to 2021. Overall, post-monsoon expansion exceeded that of pre-monsoon in all districts. Discrepancies were evident in both seasons in 2021. The applied techniques proved reliable and innovative, ensuring accurate surface water extent mapping. The GEE platform facilitated enhanced access to satellite data, significantly expediting processing through machine learning algorithms. The findings of this study have the potential to inform surface water planning and management, offering valuable insights for efficient resource utilization.

Key words: GEE platform, Northeast India, Random Forest classifier, remote sensing, Sentinel-2, surface water

HIGHLIGHTS

- Surface water extraction using multiple indices and Random Forest classifier in the Google Earth Engine platform.
- Maximum water gain was observed in Bishnupur by 6% during pre- and post-monsoon 2016.
- Maximum water loss was 7% in Bishnupur district for pre-monsoon during 2016 and 2021.
- Random Forest classifier yields satisfactory surface water extraction results compared to the Otsu thresholding method.

GRAPHICAL ABSTRACT

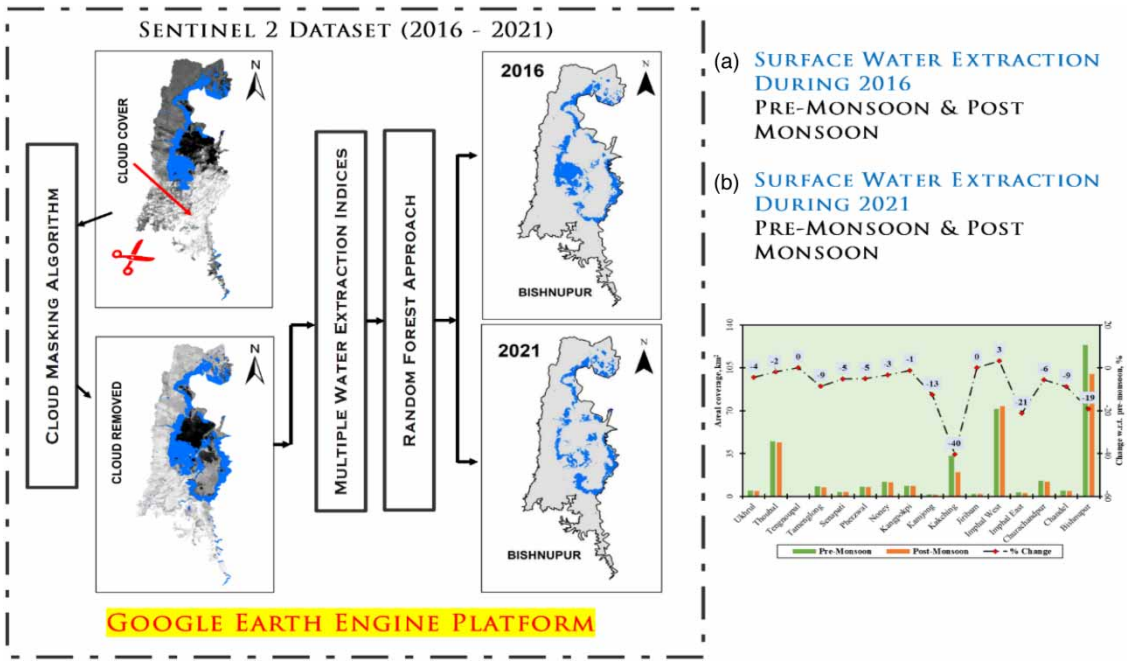

1. INTRODUCTION

Surface water refers to water bodies such as ponds, lakes, rivers, and reservoirs (Liao *et al.* 2014). It is a valuable natural resource that supports human well-being through various uses such as domestic water, irrigation, sanitation, dam power generation, navigation, and industrial operations (Vörösmarty *et al.* 2000; Lepcha *et al.* 2021). Water, a vital natural resource, undergoes transformations influenced by climate change and various environmental and social factors (Rokni *et al.* 2016). Surface water plays a crucial role in hydrological, energy, and carbon cycles (Papa *et al.* 2023). Waterbody changes affect natural resources, assets, and the environment. Its fluctuations can have various consequences, including the potential for flooding, water scarcity, and other environmental impacts. Therefore, detecting, mapping, quantifying, and monitoring surface water are vital for adequate water reserve supervision and disaster preparedness (Huang *et al.* 2018). This means supervising its changing aspects on time is crucial for informing policy and decision-making strategies.

Surface water undergoes spatial and temporal fluctuations due to aspects such as environmental change, variations in land use land cover (LULC), and ecological shifts worldwide (Karpatne *et al.* 2016; Nyatuame *et al.* 2020). Consequently, an academic investigation has extensively focused on surface water monitoring for many years (Teklu *et al.* 2015; Park *et al.* 2017; Yang *et al.* 2017; Li *et al.* 2021a; Saghafi *et al.* 2021; Tran *et al.* 2022; Jiang *et al.* 2023). The rise and fall in surface water can trigger disasters, including floods, water scarcity in arid regions, and outbreaks of waterborne diseases, resulting in human casualties (Nguyen *et al.* 2022). As a result, timely monitoring of surface water changing aspects and data dissemination are essential for disaster prevention, mitigation strategies, and decision-making (Tralli *et al.* 2005; Giardino *et al.* 2010; Liu *et al.* 2013; Zhang *et al.* 2018; Sogno *et al.* 2022).

Understanding the dynamic nature of surface water is vital due to its susceptibility to changes over time and across different regions, driven by factors such as climate variations and LULC shifts (Palmer *et al.* 2015; Lepcha *et al.* 2024). This holistic perspective highlights the intricate features of the Earth's surface, prompting extensive research efforts in monitoring surface water dynamics, including significant contributions from several researchers (Lake 2003; Klein *et al.* 2015; Teklu *et al.* 2015; Feng *et al.* 2016; Park *et al.* 2017; Wang *et al.* 2023). Moreover, changes in surface water can give rise to disasters, including floods, water shortages in arid areas, and occurrences of waterborne health, potentially harming human beings (Feyisa *et al.* 2014). Nowadays, remote sensing data with different spatio–temporal and spectral capabilities have become indispensable to observe dynamic information related to Earth's various resources, particularly surface water.

Various mathematical models for surface water extraction have been established using existing data, remote sensing, and geographic information system (GIS)-based methodologies applied to observational datasets. Moreover, remote sensing and GIS-based approaches used for Earth observational datasets are now among the most widely used strategies. Rapid data may be retrieved, continually monitored, and analyzed to demonstrate various land resources at the lowest possible expense. Using remote sensing technology and methodologies, surface water supervision has been the most engaged pursuit throughout history. Traditionally, surface water mapping relied on visual analysis of satellite images from different periods. However, this approach faced challenges in maintaining continuity across chronological data series, making it hard to outline the extent due to seasonal pattern variations accurately (Mohammadi *et al.* 2017). Subsequently, numerous automated procedures were presented to extract surface water to address the abovementioned issues. These approaches utilize satellite imagery that exhibits diverse spatial and spectral attributes. These attributes encompass perceptron models, neural networks with multilayer perceptron (Balázs *et al.* 2018), entropy-driven techniques (Horkaew & Puttinaovarat 2017), extraction of spatial and spectral sub-pixel information through regression models (Kaplan & Avdan 2017), band-ratio analysis (Xu 2006; Singh *et al.* 2015; Deng *et al.* 2020), the fusion of density slicing with Hue, Intensity, and Saturation (HIS) transformation (Frazier & Page 2000), decision tree algorithms (Acharya *et al.* 2016; Olthof 2017), image segmentation, and pattern recognition (Chen *et al.* 2014; Xie *et al.* 2016a, 2016b).

Sentinel-2 is the second satellite in the European Commission and European Space Agency Copernicus program, providing global land surface multi-spectral photography with better spatio–temporal resolution. Sentinel-2 images demonstrate higher accuracy regarding water extraction through indices, particularly in delineating water bodies. The red, blue, green, and near-infrared (NIR) bands of the sensor have a 10 m spatial resolution, but the two shortwave infrared (SWIR) bands, which are often used for water index, have a 20 m resolution, somewhat reducing water extraction accuracy. The Normalized Difference Water Index (NDWI), which uses green and NIR bands with a 10 m ground resolution, showed significant misclassification errors, whereas the band sharpening approach achieved 10 m water precision but had a lengthy computation time. Li *et al.* (2021b) used four 10 m and two 20 m SWIR bands from Sentinel-2 for surface water mapping at 10 m resolution using Support Vector Machine (SVM). However, due to the small size of the training sample, the Multi-Spectral Water Index is challenging to apply universally.

Water extraction and monitoring through remote sensing leverage optical and radar data, primarily sourced from Earth observation satellites. Recent advancements focus on enhancing spatial, temporal, and spectral resolutions in data obtained from remote sensing of water bodies (Yan & Jinwei 2019). Optical imagery, a component of passive remote sensing, currently serves as the primary data source for extracting water body information due to distinctive low reflectivity in visible and NIR ranges and extremely low reflectivity in NIR and SWIR spectra. While diverse spatial resolution remote sensing data exists, fine resolution imagery such as Landsat and Sentinel has gained prominence for its increased accuracy.

Selecting optimal sensors is crucial for acquiring ground information, and often, a combination of two or more sources is preferred for water body extraction. Optical sensors offer eminent spatial and spectral resolution but are susceptible to cloud and shadow interference during water recognition. Synthetic aperture radar (SAR) images have some natural disruption, but they are still helpful for locations with shallow water and shadows. Combining textural features is one way to reduce the influence of noise, but it takes a lot of work and constant testing to find the best feature blend (Zhu *et al.* 2006). Furthermore, digital surface models and digital elevation models are important for water body estimates because they use terrain factors to reduce shadow interference and eliminate missing water bodies (Horkaew & Puttinaovarat 2017; Li *et al.* 2018).

In advancing the understanding of surface water dynamics, Yang *et al.* (2020) contributed insights by applying a rule-based superpixel approach on Sentinel-2 data, showcasing the integration of spectral index and superpixel techniques without training data, enhancing precision in surface water mapping. Halder *et al.* (2023) conducted a case study on flood hazard monitoring in Assam, India, using Google Earth Engine (GEE). They used Sentinel-2 data for landscape impact assessment, and Landsat 8 datasets for modified NDWI (MNDWI) within the GEE platform aligns with the scope of advancing methodologies in surface water dynamics. Dehkordi *et al.* (2022) examined spatiotemporal changes in Iran's surface water using Landsat data on GEE, highlighting the superiority of NIR-based water mapping rules in arid regions. Atay & Kaplan (2023) mapped Turkish inland water using a Multi-Band Water Index. Kandekar *et al.* (2021) analyzed the Jayakwadi dam in India, utilizing NDWI to monitor surface water dynamics within the scope of advancing methodologies. Li *et al.* (2022) contributed a review emphasizing the importance of higher spatial resolution data in analyzing surface water dynamics. Chen & Zhao (2022) demonstrated advances in surface water exploration by employing Sentinel-1 and Sentinel-2 data, achieving >96% overall accuracy. Singh (2022) utilized a SAR to analyze floods in Manipur, adding valuable insights to the scope of surface water dynamics. Sur *et al.* (2021) estimated Punjab's surface water dynamics using Sentinel-2, showcasing the effectiveness of the MNDWI.

Previous studies primarily focused on automated extraction and the utilization of single water indices, as discussed previously. In contrast, this study employs the delineation of surface water using multiple water indices in conjunction with the Otsu threshold and a Random Forest (RF) classifier for decision-making. Frequently, a synergistic approach involving both water indices and machine learning is adopted to achieve comprehensive and accurate results.

Various approaches have been exploited for extracting surface water such as density slicing in which an individual infrared (IR) band obtains a water map (Frazier & Page 2000). Alternatively, both supervised and unsupervised classification techniques (Ozesmi & Bauer 2002) generate LULC maps, from which the extent of water is obtained. Decision trees, utilizing multi-spectral bands, have also been employed for water delineation (Acharya *et al.* 2016), but the difficulty hinders their universal applicability in constructing robust classification rules.

A more effective approach involves using water indices calculated from multiple bands to discern contrasts between water and non-water bodies. Numerous indices, such as the Tasseled Cap Wetness Index (Crist 1985), Normalized Difference Vegetation Index (NDVI), and others, have been developed for this purpose. Notably, the NDWI (Mcfeeters 1996) and MNDWI (Xu 2006) have gained prominence. The MNDWI, replacing the NIR band with SWIR, proves more stable and reliable due to SWIR's reduced sensitivity to optical constituents within the water. However, caution is advised in snow-covered regions, where the normalized difference snow index might be more suitable.

The critical issue of thresholding in water index applications is addressed through various approaches. While a threshold of 0 is commonly applied, studies suggest that adjusting the threshold value enhances extraction results (Ji *et al.* 2009). Automation challenges arise when thresholding time series or single images covering multiple water bodies, prompting the development of automated methods. Li & Sheng (2012) proposed an adaptive thresholding scheme, later applied to MNDWI by Allen & Pavelsky (2015). Feyisa *et al.* (2014) pioneered the Automated Water Extraction Index (AWEI), offering a single-threshold solution for water detection from time series Landsat imagery, while Fisher *et al.* (2016) presented the WI2015 index, demonstrating comparable strength to existing water indices.

In Manipur, despite ample monsoon rainfall, water scarcity persists for agriculture, drinking, and domestic use due to inadequate management, ultimately affecting the rivers and ecological balance of the region. Most districts rely on surface water and groundwater, covering only 1.65% of the land area. Surface sources such as wetlands, lakes, ponds, and rivers are insufficient for sustainable development. Deforestation and shifting cultivation have led to the depletion of springs in hilly areas, further worsening the situation. These water sources are vital for economic and social development and environmental integrity. Some regions experience persistent water shortages, even during the monsoon, while valley districts face recurrent floods, causing damage. Improved water resource management is urgently needed for sustainable development and ecological preservation in Manipur.

The uniqueness of this study is to analyze the surface water dynamics in Manipur, especially during pre- and post-monsoon season extending from 2016 to 2021, using the Sentinel-2–2 data with the state-of-the-art approach in the GEE platform. Notably, no similar studies have been conducted in the region before. The study holds promise for providing fresh perspectives on surface water dynamics, seasonal fluctuations, and their significance for water resource management in Manipur. Furthermore, it may present inventive solutions and policy suggestions for addressing water scarcity challenges efficiently.

Tackling the growing scarcity of water resources intensified by climate change and human activities requires immediate attention. A crucial aspect of effective water conservation involves the thoughtful and sustainable management of water sources, necessitating consistent monitoring, mapping, and evaluation of water bodies. Conventional methods for updating national water maps often present challenges, but recent advancements in remote sensing provide viable solutions. In this study, we utilized remote sensing data integrated into GEE to develop an application for mapping the inland water bodies of the Northeast Indian state of Manipur. Based on the above discussion, the primary aims of this study are (1) to extract the surface water spread-out area of the selected districts of Manipur. (2) To analyze seasonal surface water changes during 2016 and 2021 in selected districts of Manipur. To achieve this objective, we explored different surface water extraction indices within GEE, capitalizing on Sentinel-2 satellite imagery and applying it comprehensively across the research area.

2. MATERIALS AND METHODS

2.1. Study area

The state of Manipur lies in the northeastern part of India and shares an international border with Myanmar to the south–east part. The study area comprises about 90% of hilly regions and the rest, about 10% of valley regions, extending from 23.8° to

25.7° N to 92.9 to 94.7° E, encircling a total area of 22,327 km^2. Administratively, Manipur is divided into 16 districts, namely Bishnupur, Chandel, Churachandpur, Imphal East, Imphal West, Jiribam, Kakching, Kamjong, Kangpokpi, Noney, Pherzawl, Senapati, Tamenglong, Tengnoupal, Thoubal, and Ukhrul (Figure 1). Six of the districts, namely Bishnupur, Thoubal, Imphal East, Imphal West, Jiribam, and Kakching, are valley regions whereas the rest are hilly. As of the 2011 census, Manipur had a population of approximately 2.7 million, with a growth rate of 12.05%. Over 64% of the state is covered in natural vegetation and receives an annual rainfall of 1,657.6 mm. The primary rivers in Manipur include the Imphal River, Iril, Nambol, Thoubal, Sekmai, Wangjing, Khuga, and Chakpi. The state's drainage system comprises various streams connected to the Manipur River and its tributaries, in addition to smaller streams and associated lakes that form the valley's water resources. During the monsoon months (May–September), a catchment area spanning 6,332 km^2, accounting for approximately 28.4% of the state's total area, discharges a significant volume of water into the Manipur River system, often leading to periodic inundation of land along their banks. The geographical attributes of the study area are provided in Table 1.

2.2. Data collection

Sentinel-2, part of the Copernicus Land Monitoring program, has higher spatial resolution multi-spectral imaging capabilities designed for monitoring various aspects of the Earth's surface, including vegetation, soil, water bodies, and coastal areas. It comprises two main satellites, Sentinel- 2A and 2B, offering a rapid revisiting cycle of about 5 days. Sentinel-2 has a multi-spectrometer featuring 13 spectral bands covering the visible, NIR, and SWIR ranges. To extract surface water automatically, cloud-free images from the database are selected based on a thresholding technique outlined in the product algorithm (Richter *et al.* 2012). This procedure ensures the inclusion of high-quality data less than 10% cloud. An extensive 5-year database to average seasonal surface water dynamics was used. The specifications of the data used are provided in Table 2.

2.3. Selection of database for analysis

The methodology is presented in Figures 2–4, comprising three main steps: (i) database selection, (ii) surface water extraction algorithm, and (iii) evaluation and accuracy assessment, which are explained in detail below.

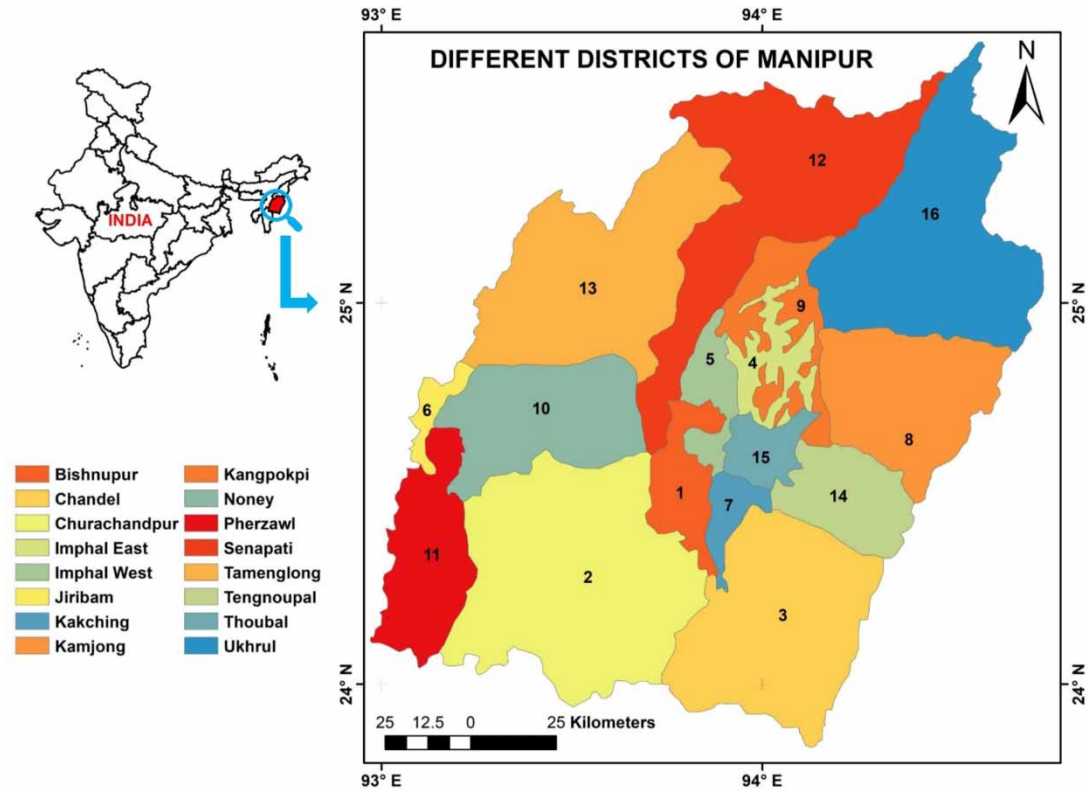

Figure 1 | Study area showing different districts of Manipur.

Table 1 | Location details of the selected districts of Manipur

Sl.	Districts	Latitude (°N) & Longitude (°E)		Avg. elevation (m amsl)
		Upper/left	Lower/right	
1	Bishnupur	24.28, 93.69	24.75, 93.91	828
2	Churachandpur	23.94, 93.15	24.62, 93.86	914
3	Chandel	23.84, 93.73	24.47, 94.32	790–3,050
4	Imphal East	24.67, 93.90	25.07, 94.14	790
5	Imphal West	24.54, 93.78	24.99, 93.94	790
6	Jiribam	24.55, 93.07	24.85, 93.25	252
7	Kakching	24.24, 93.85	24.56, 94.03	776
8	Kamjong	24.47, 93.15	24.94, 94.65	1,535
9	Kangpokpi	24.62, 93.87	25.18, 94.19	992
10	Noney	24.48, 93.14	25.87, 93.69	41
11	Pherzwal	24.04, 92.97	24.67, 92.25	1,037
12	Senapati	24.60, 93.67	25.61, 94.48	1,061–1,788
13	Tamenglong	24.78, 93.21	25.45, 93.95	1,580
14	Tengnoupal	24.33, 94.02	24.65, 94.39	760–3,050
15	Thoubal	24.51, 93.89	24.73, 94.15	790
16	Ukhrul	24.87, 94.12	25.68, 94.74	3,114

Table 2 | Sentinel-2 data specification

Bands	Ground resolution, m	Wavelength, μm
B2 (Blue)	10	0.490
B3 (Green)		0.560
B4 (Red)		0.663
B8 (NIR)		0.842
B11 (SWIR1)	20	1.610
B12 (SWIR2)		2.190

GEE is an open cloud platform for processing and analyzing geoscience data (Gorelick *et al.* 2017). This platform primarily stores satellite and Earth surveillance data while offering ample processing power for data transfer and processing, in contrast to conventional image processing software and Environment for Visualizing Images (ENVI) and Earth Resource Data Analysis System (ERDAS). GEE excels at rapid batch image processing, delivering analysis results without the need for image data downloads. The platform supports both an online JavaScript API and an offline Python API, facilitating the swift creation of web services via Google Cloud by utilizing these APIs.

The Sentinel-2 data from 2016 to 2021 underwent de-clouding and radiometric calibration processes. Cloud removal employs two methods: image-based cloud sorting and a pixel-based GEE algorithm. The former method opts for imageries with less than 30% cloud cover, while the latter calculates per-band percentile values from the pixels with the lowest cloud scores. Thus, the second approach prefers scenes with minimal cloud cover in areas with more scenes than the specified maximum limit. However, a drawback of this method is the persistence of visible residues around removed cloud patches, potentially affecting water extraction processes.

2.4. Algorithm for extracting surface water bodies

The surface water extraction involved employing key algorithms, including the NDWI, MNDWI, NDVI, and the AWEI. NDWI, focusing on the green and NIR bands, and MNDWI, emphasizing the green and SWIR bands, played crucial roles

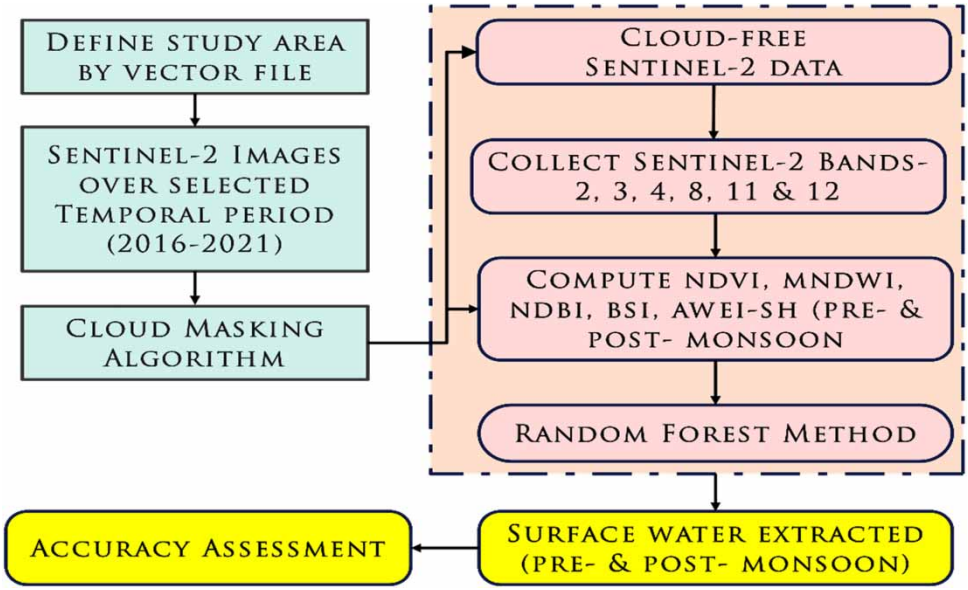

Figure 2 | Methodology for surface water extraction using Sentinel-2 images.

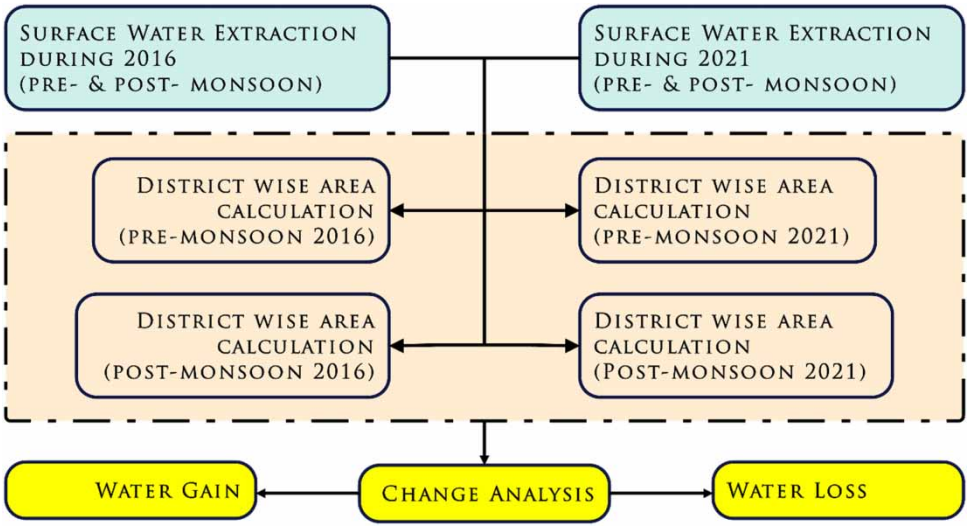

Figure 3 | Methodology for seasonal surface water change analysis during 2016 and 2021.

in capturing spectral distinctions between water and non-water features. AWEI specifically addressed shadow effects, enhancing overall water extraction accuracy. Additionally, supervised classification utilized machine learning for pixel categorization, with a set of known land cover types training the algorithm. The application of RF regression, a robust technique, facilitated efficient surface water mapping, especially adept at handling large datasets. These combined methodologies ensured a comprehensive and precise mapping of surface water extent in the study area.

2.5. Surface water extraction indices

The Earth's surface presents a diverse array of aquatic and terrestrial landforms, each characterized by unique complexities. Surface water features, including rivers, lakes, reservoirs, and seas, exhibit distinct shapes and spectral profiles. Conversely, non-water elements such as shadows, roads, and buildings may share spectral and spatial similarities, introducing potential

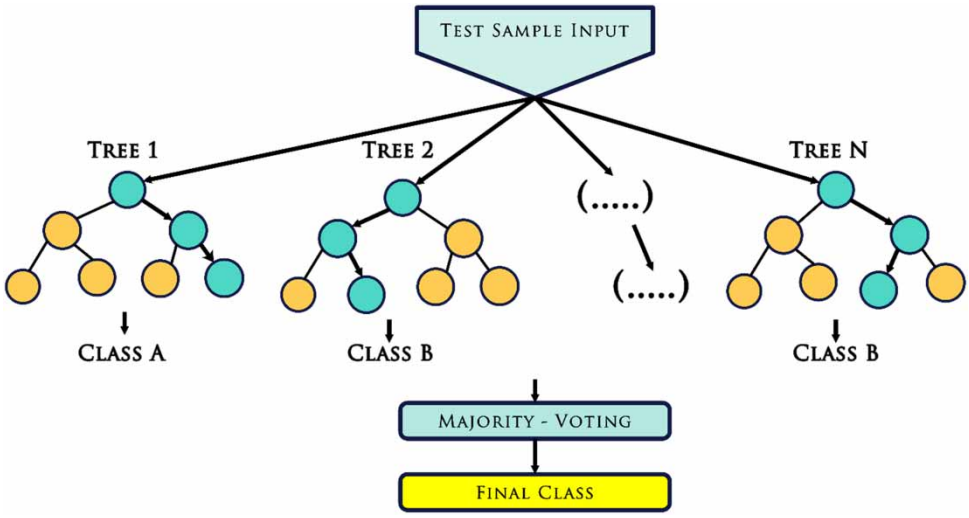

Figure 4 | RF regression sample structure.

confusion with actual water bodies. Consequently, achieving precise identification of water bodies remains imperative despite these challenges.

Optical image-based surface water extraction takes advantage of the lower reflectance of water, particularly in IR channels, compared to other LULC types. Various techniques tailored for this purpose have emerged in optical remote sensing imagery. A practical methodology involves computing water indices from multiple bands to discern contrasts between water and non-water bodies. In this study, we employed several methods – such as NDVI, MNDWI, AWEI, supervised classification, and RF regression – to map the extent of surface water.

The application of water indices and machine learning techniques offers a more objective, efficient, and scalable solution compared to conventional approaches such as visual interpretation or manual delineation. These advanced methods accurately manage large datasets, providing quantitative outputs that mitigate subjectivity and enhance study repeatability. The decision to employ these water indices is justified by their effectiveness in harnessing the spectral characteristics of surface water in optical remote sensing imagery. The integration of multiple indices and machine learning demonstrates a comprehensive and robust strategy for surface water extraction. The selection of indices and methods is justified by their sensitivity to water features, capacity to address common challenges in surface water extraction, and alignment with optical remote sensing capabilities. This approach represents a more sophisticated and objective method for studying surface water extraction compared to certain traditional methods. The different water extraction indices tested are defined in the following equation:

$$\mathrm{NDVI} = \frac{\mathrm{NIR} - \mathrm{Red}}{\mathrm{NIR} + \mathrm{Red}} \tag{1}$$

The NDVI measures greenness or density by assessing reflectance in the red and NIR spectrum. In the event of healthy vegetation, more visible light will be noticed, as well as greater NIR reflectance, whereas, in the case of unhealthy vegetation, the opposite will be observed. A high NDVI rating indicates that the vegetation is healthy and dense. The lower the NDVI number, the sparser the vegetation. It is probably grassland or desert, if only a slight change in reflectance between visible and NIR. NIR radiation minus visible red divided by NIR and visible red yields the NDVI, which will be used to determine vegetation. NDVI has a range of -1 to $+1$. There is no vegetated area if the index value is 0 to -1, and there is a vegetated area if the index value is 0 to 1

$$\mathrm{MNDWI} = \frac{\mathrm{Green} - \mathrm{SWIR1}}{\mathrm{Green} + \mathrm{SWIR1}} \tag{2}$$

The MNDWI is the modified NDWI (Xu 2006), which has improved accuracy, particularly in urban water extraction. The MNDWI boosts the visibility of open water features while efficiently reducing unwanted elements such as built-up, vegetation, and soil interference. Its superiority over the NDWI lies in its capacity to significantly diminish or eliminate built-up land noise, making it a preferred choice for enhancing and extracting water information in regions where built-up land dominates the background.

$$\text{AWEI} - \text{sh} = \text{Blue} + 2.5 \times \text{Green} - 1.5\,(\text{NIR} + \text{SWIR1}) - 0.25 \times \text{SWIR2} \tag{3}$$

The AWEI was introduced by Feyisa *et al.* (2014) to locate water features for particularly complicated locations and to overcome shadow problems in hilly terrain. It has two conditions: AWEI-sh is for removing shadow pixels, but AWEI-sh is for locations with an urban background. The AWEI was created to increase classification accuracy in shadow and dark surfaces, frequently misclassified by conventional classification approaches. Moreover, various indices for various sensors and locations have been developed by diverse research with differing degrees of accuracy.

2.6. Supervised classification

The predominant approach for quantitatively analyzing remote sensing image data is supervised classification. This method entails identifying spectrally similar areas in an image using known target 'training' sites and applying their spectral signatures to unknown target areas. It necessitates using specific, homogeneous training data and implementing techniques or decision rules.

In order to instruct the computer to identify comparable patterns within imagery accurately, it necessitates high-quality training data. This constitutes only a fraction of the entire image or region to be classified. In this research, training samples were sourced from a notably high-resolution Google Earth Pro dataset, ranging from 15 cm to 15 m, to curate diverse classes for the training dataset. Approximately 100 sample points were gathered for each class to facilitate algorithm training. Additionally, field visits were conducted to validate the precision of the chosen training dataset.

The goal is to provide a quantitative description of how each thematic (LULC) class in the image appears. The purpose is to select numerous regions throughout the image for each LULC category. The type of training data used can substantially impact the classification outcomes. The first step must thus be determining the classes of interest, which necessitates careful consideration of the study's goal.

2.7. Random Forest method

RF is a combined procedure developed based on a decision tree classifier. Using the bagging resampling method, multiple samples are removed from the original dataset, and for each bagging, the sample creates decision trees, and as the final output, it estimates the mean estimate of all decision trees. They overfit their training set when trees are full-grown and likely to learn extremely uneven patterns; it has significant variance but a small bias. RF is a method of averaging numerous deep decision trees, and the same training was done on different parts of the dataset, aiming to reduce variance. In the RF algorithm, every selected decision tree of the samples randomly generates the tree nodes.

2.8. Accuracy assessment

This study employed a rigorous pixel-level analysis to assess the accuracy of a map, treating each pixel as an independent unit. We utilized an error matrix (confusion matrix) to identify and pinpoint misclassifications at specific locations, providing detailed insights beyond just overall accuracy. By analyzing both diagonal and off-diagonal elements, we gained a valuable understanding of the classifier's performance for each class, including both commission and omission errors. Additionally, we employed further metrics such as overall accuracy (OA), which measures the overall correctness of a classification, producer's accuracy (PA) measures the percentage of correctly categorized pixels for a specific class in the reference data, user's accuracy (UA) indicates how reliably a class on the map corresponds to the actual presence of that class on the ground, and the Kappa coefficient (K) assesses the agreement between two rasters, each classifying items into mutually exclusive

categories. The following equation defines all the parameters for accuracy assessment:

$$\text{OA} = \frac{\text{Number of accurate pixels}}{\text{Total number of pixels}} \tag{4}$$

$$\text{PA} = \frac{\text{Number of correctly classified pixels}}{\text{Total number of pixels in the reference map}} \tag{5}$$

$$\text{UA} = \frac{\text{Number of correctly identified pixels}}{\text{Total number of pixels in classified map}} \tag{6}$$

$$K = \frac{(T \times C) - G}{T^2 - G} \tag{7}$$

where T represents the test pixels, C denotes the correctly classified pixel observations, and G signifies the sum of multiplied total values. When both rasters are in complete agreement, K equals 1. On the other hand, when there is no alignment between the raster data, the coefficient K equals 0. K-values exceeding 0.75 are deemed excellent, those falling within the range of 0.40–0.75 are classified as fair to good, and values below 0.40 are seen as poor.

3. RESULTS

3.1. Accuracy evaluation using multiple matrices

The accuracy of the surface water mapping using the water indices was assessed over designated periods in different districts of Manipur. The PA, OA, and K coefficients calculated during the selected period from 2016 to 2021 for both pre-monsoon (PrM) and post-monsoon (PoM) seasons are listed in Table 3. The results suggest higher accuracy in mapping surface water extent over different districts of Manipur. The OA was found greater than 97% (minimum at Thoubal), PA with greater than 91% (minimum observed at Thoubal during pre-monsoon), UA with minimum of 93%, and above (minimum observed at Bishnupur during post-monsoon), and the minimum Kappa value with 0.96 at Thoubal (pre-monsoon) and Bishnupur (post-monsoon).

Table 3 | Accuracy assessment of selected study areas for pre- and post-monsoon from 2016 to 2021

		OA (%)		PA (%)		UA (%)		K	
Sl.	District	PrM	PoM	PrM	PoM	PrM	PoM	PrM	PoM
1	Bishnupur	98	97	100	100	95	93	0.97	0.96
2	Chandel	98	99	100	95	100	100	0.97	0.99
3	Churachandpur	100	100	100	100	100	100	1	1
4	Imphal East	98	99	100	100	100	100	0.98	0.99
5	Imphal West	99	98	100	100	100	100	0.98	0.98
6	Jiribam	99	99	100	100	100	100	0.99	0.98
7	Kakching	99	99	100	100	100	96	0.99	0.99
8	Kamjong	98	99	100	100	100	100	0.97	0.99
9	Kangpokpi	99	100	100	100	100	100	0.99	1
10	Noney	100	99	100	100	100	100	1	0.99
11	Pherzwal	98	98.9	100	100	100	100	0.98	0.98
12	Senapati	99	98	100	100	96	98	0.99	0.98
13	Tamenglong	100	98	100	100	100	100	1	0.98
14	Tengnoupal	98	98	100	100	100	100	0.98	0.97
15	Thoubal	97	98	91	97	97	100	0.96	0.98
16	Ukhrul	100	100	100	100	100	100	1	1

3.2. Surface water spread in selected districts of Manipur

Out of the various districts in Manipur that were examined, only four districts, namely Bishnupur, Imphal West, Kakching, and Thoubal, exhibit extensive surface water networks. Yet, there are significant variations in the distribution of surface water between the pre-monsoon and post-monsoon seasons. The remaining districts possess limited networks of lakes, rivulets, and rivers. Table 4 and Figure 5 (substantial coverage) present the surface water coverage in different Manipur districts during the periods of pre-monsoon and post-monsoon from 2016 to 2021, respectively. The small surface water coverage (12 districts) in the remaining districts is provided in Supplementary Materials (Fig. A1).

The surface water spreads in valley regions more than in hilly regions. Among the different districts of Manipur, the highest surface water area was observed at Bishnupur district during pre- and post- monsoon throughout the study period of 5 years where Loktak Lake is located. The second-highest surface water area was observed in Imphal West, and the lowest surface water spread was obtained at the Tengnoupal district, a hilly region of Manipur (Figure 6). It is worth mentioning here that only a single district (Imphal West) has shown a slight increase in areal coverage of surface water. All other districts have shown a slight decrease in area coverage of surface water, while four districts in central and northern Manipur, namely Kamjong, Bishnupur, Imphal East, and Kakching, have shown a substantial decrease by 13, 19, 21, and 40%, respectively.

3.3. Quantitative change analysis evaluation of surface water extraction results

During 2016, it was observed that the actual areal coverage of water bodies increased during post-monsoon with reference to pre-monsoon season except in Imphal West district, which decreased by 4.66 km^2. On the other hand, a substantial increase was observed in Bishnupur and Kakching districts by 4.61 and 8.39 km^2. Similarly, during 2021, a considerable increase in water bodies was observed at Bishnupur and Imphal West district by 6.49 and 13.69 km^2 from pre-monsoon to post-monsoon season. The remaining stations have shown a small decrease, with a maximum of 1.65 km^2 at Churachandpur. Table 5 shows the quantitative surface water available in different districts of Manipur during pre- and post-monsoon during 2016 and 2021.

The change in water bodies from 2016 to 2021 during post-monsoon season revealed that substantial gain and loss were observed in Bishnupur, Imphal West, and Kakching districts. Bishnupur gained 19 km^2 from and lost 30 km^2 to non-water bodies; Imphal West and Kakching gained 18 and 13 km^2 from and lost 26 and 30 km^2 to non-water bodies. Relatively, only the Thoubal district has lost its water bodies by 19 km^2. It is worth mentioning that the overall change in water bodies during post-monsoon season from 2016 to 2021 revealed that the loss in areal coverage of water bodies is relatively

Table 4 | Surface water spread in different districts of Manipur

		Extracted surface water area (2016–2021), km^2	
Sl.	District	Pre-monsoon combined	Post-monsoon combined
1	Bishnupur	123.62	100.03
2	Chandel	4.61	4.23
3	Churachandpur	12.71	11.96
4	Imphal East	3.34	2.56
5	Imphal West	71.54	73.80
6	Jiribam	2.00	1.98
7	Kakching	33.41	19.92
8	Kamjong	1.55	1.43
9	Kangpokpi	8.56	8.49
10	Noney	12.03	11.61
11	Pherzwal	8.00	7.61
12	Senapati	3.76	3.58
13	Tamenglong	8.14	7.42
14	Tengnoupal	0.24	0.21
15	Thoubal	44.95	44.24
16	Ukhrul	4.46	4.31

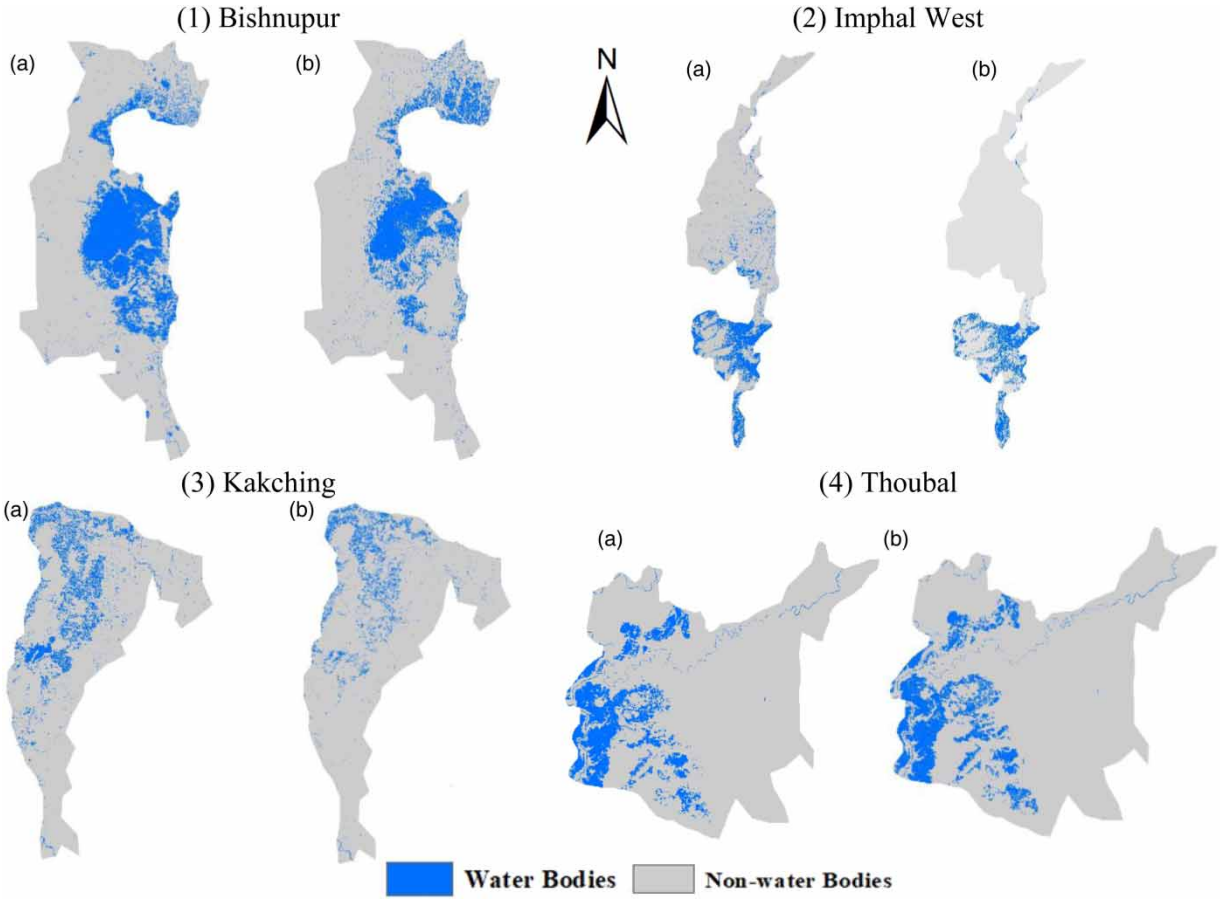

Figure 5 | Significant surface water spread in combined (a) pre-monsoon 2016 and (b) post-monsoon 2021 at different districts of Manipur at (1) Bishnupur, (2) Imphal West, (3) Kakching, and (4) Thoubal.

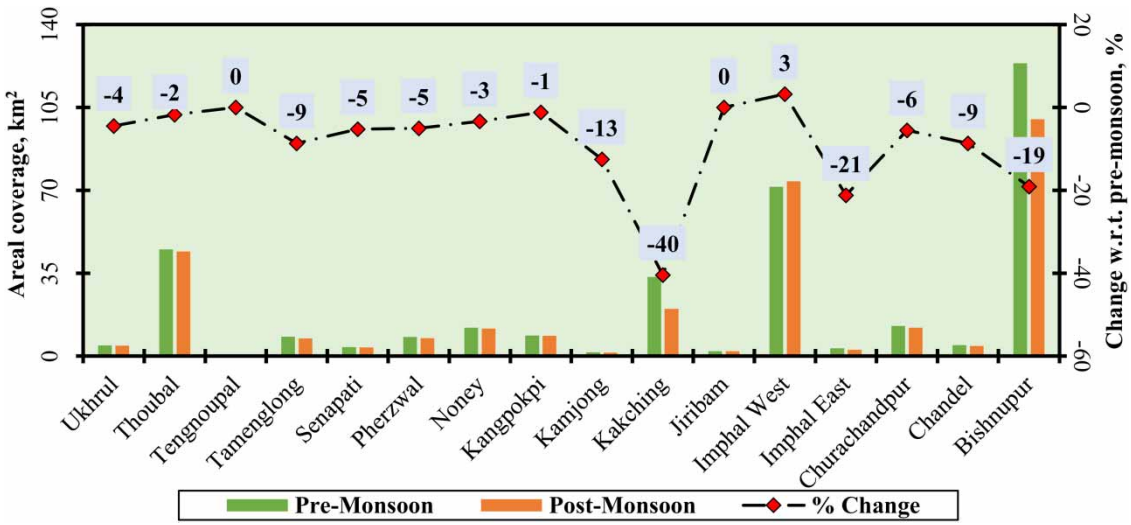

Figure 6 | District-wise area of surface water spread during pre- and post-monsoon in selected districts of Manipur.

Table 5 | Quantitative surface water spread pre- and post-monsoon for 2016 and 2021

		Extracted surface water bodies, km²			
Sl.	District	PrM 2016	PoM 2016	PrM 2021	PoM 2021
1	Bishnupur	132.78	137.39	121.44	128.38
2	Chandel	4.79	4.86	4.32	4.12
3	Churachandpur	12.71	13.20	11.96	10.31
4	Imphal East	3.17	3.29	2.75	2.55
5	Imphal West	86.70	82.04	60.71	74.40
6	Jiribam	2.01	2.12	1.94	1.89
7	Kakching	32.70	41.09	23.96	24.11
8	Kamjong	1.54	1.58	1.51	1.42
9	Kangpokpi	8.48	8.58	8.38	8.22
10	Noney	11.55	12.45	11.12	11.07
11	Pherzwal	7.90	7.96	6.96	6.75
12	Senapati	3.53	4.15	2.83	2.58
13	Tamenglong	8.24	9.08	7.28	6.96
14	Tengnoupal	0.20	0.24	0.17	0.16
15	Thoubal	42.68	48.28	41.21	29.56
16	Ukhrul	4.59	4.68	4.07	3.23

higher than gain, which shows a trend towards the water scarcity scenarios in all districts of Manipur. Overall, the change in the remaining district was very small, as shown in Table 6.

During the year 2016, from pre- to post-monsoon season, a resultant gain in water bodies was (relatively higher than loss) observed at Bishnupur, Kakching, and Thoubal districts by 11, 8.5 and 6 km^2 while only Imphal West lost about 5 km^2 to non-water bodies. In general, the change in the remaining district was very small and negligible, as shown in Table 7.

Table 6 | District-wise change in surface water area (km^2) during post-monsoon 2016 and post-monsoon 2021

Sl.	District	Non-water bodies	Water gain	Water loss	Water bodies
1	Bishnupur	409.39	19.10	30.00	102.26
2	Chandel	2,477.51	0.28	1.02	3.84
3	Churachandpur	3,497.31	1.91	3.15	10.05
4	Imphal East	389.09	0.79	0.99	1.75
5	Imphal West	342.48	18.08	25.72	56.31
6	Jiribam	171.99	0.12	0.35	1.77
7	Kakching	203.09	13.40	30.38	10.71
8	Kamjong	1,673.27	0.21	0.37	1.21
9	Kangpokpi	800.42	0.47	0.84	7.75
10	Noney	1,506.20	1.48	2.86	9.59
11	Pherzwal	1,117.77	0.42	1.63	6.34
12	Senapati	2,787.55	0.34	1.91	2.24
13	Tamenglong	2,641.14	1.13	3.24	5.84
14	Tengnoupal	841.36	0.08	0.16	0.08
15	Thoubal	308.27	0.70	19.43	28.85
16	Ukhrul	2,820.19	0.94	2.39	2.29

Table 7 | District-wise change in surface water area (km^2) during pre-and post-monsoon 2016

Sl.	District	Non-water bodies	Water gain	Water loss	Water bodies
1	Bishnupur	399.06	34.94	23.96	93.73
2	Chandel	2,477.04	0.79	0.71	4.08
3	Churachandpur	3,499.28	0.49	0.00	12.71
4	Imphal East	388.61	0.80	0.68	2.49
5	Imphal West	332.45	23.46	28.11	58.58
6	Jiribam	171.82	0.39	0.28	1.73
7	Kakching	197.31	27.56	19.16	13.53
8	Kamjong	1,673.37	0.14	0.10	1.44
9	Kangpokpi	800.41	0.56	0.46	8.02
10	Noney	1,505.95	2.63	1.73	9.82
11	Pherzwal	1,116.81	1.42	1.36	6.54
12	Senapati	2,787.37	1.11	0.49	3.04
13	Tamenglong	2,640.70	2.38	1.55	6.70
14	Tengnoupal	841.37	0.12	0.08	0.12
15	Thoubal	302.88	11.70	6.10	36.58
16	Ukhrul	2,819.78	1.44	1.35	3.24

During the pre-monsoon season from 2016 to 2021, it was revealed that substantial loss in water bodies was observed in Bishnupur, Churachandpur, Imphal West, Kakching, and Ukhrul districts. They lose about 11.4, 2.77, 25.98, 8.74, and 1.47 km^2 to non-water bodies. Overall, it is observed that the areal coverage of surface water bodies in all districts of Manipur is losing to non-water bodies during pre-monsoon season from 2016 to 2021, showing the way towards the water scarcity scenarios in all districts of Manipur as shown in Table 8.

Table 8 | District-wise change in surface water area (km^2) during pre-monsoon of 2016 and 2021

Sl.	District	Non-water bodies	Water gain	Water loss	Water bodies
1	Bishnupur	402.19	25.97	37.32	95.46
2	Chandel	2,477.47	0.34	0.81	3.98
3	Churachandpur	3,498.70	1.04	3.81	8.90
4	Imphal East	388.67	0.74	1.16	2.00
5	Imphal West	347.27	8.66	34.64	52.05
6	Jiribam	171.98	0.22	0.28	1.72
7	Kakching	216.78	8.11	16.85	15.85
8	Kamjong	1,673.34	0.19	0.22	1.32
9	Kangpokpi	800.06	0.94	1.05	7.44
10	Noney	1,507.09	1.51	1.93	9.62
11	Pherzwal	1,117.55	0.69	1.63	6.26
12	Senapati	2,787.63	0.88	1.58	1.95
13	Tamenglong	2,641.53	1.56	2.52	5.72
14	Tengnoupal	841.40	0.10	0.13	0.07
15	Thoubal	302.73	11.84	13.31	29.36
16	Ukhrul	2,819.89	1.34	1.86	2.73

During the year 2021, from pre- to post-monsoon season, a gain in water bodies was (relatively higher than loss) observed at Bishnupur and Churachandpur districts by 7 and 2 km^2 while Imphal West, Kakching, and Thoubal lost by about 7.6, 17, and 11.7 km^2 to non-water bodies. The changes in the remaining district were very small and negligible, as shown in Table 9. The substantial change in the extent of surface water at different districts of Manipur during (a) PoM 2016 to PoM 2021, (b) PrM 2016 to PoM 2016, (c) PrM 2016 to PrM 2021, and (d) PrM 2021 to PoM 2021 are shown in Figure 7. The small changes in surface water in the remaining districts are provided in Supplementary Materials (Fig. A2).

4. DISCUSSION

Numerous studies have applied varied methodologies for surface water extraction, showcasing notable outcomes. Rapinel *et al.* (2019) employed a support vector machine and an RF approach in the Couesnon floodplain, France, favoring the former for superior performance. Chen & Zhao (2022) devised an algorithm based on topological relationships and a digital surface model local search algorithm, achieving heightened accuracy in delineating surface water across the plain and mountainous terrains along the Yangtze River, China. Mayer *et al.* (2021) utilized a deep learning approach to map surface water over Cambodia and Southeast Asia, generating results comparable to conventional methods. Goffi *et al.* (2020) mapped flooded areas in northern Italy through soft fuzzy integration, reporting consistently greater and robust mapping accuracy. Sur *et al.* (2021) employed an MNDWI with the Otsu method, yielding promising results in western India. In our investigation, the analysis demonstrated that, under consistent conditions, the RF classifier reliably extracted surface water extent over the Otsu threshold approach.

Traditionally, global-scale studies have been the focus of surface water mapping. However, there is now a growing need for higher-resolution mapping at the regional level (Sur *et al.* 2021) to better comprehend inundation patterns and formulate effective management strategies (Laonamsai *et al.* 2023). GEE offers the computational power and analytical capabilities necessary to process Sentinel-2 datasets and generates a detailed final product with an impressive resolution of 10 m. MNDWI, NDVI, Normalized Difference Build-Up Index (NDBI), AWEI-sh, and Bare Soil Index (BSI) algorithms were used on the GEE platform to extract surface water using an RF classifier for pre- and post-monsoon seasons in this study. The backscatter coefficient's median value was used to synthesize Sentinel-2–2 images of the study region during the pre- and post-monsoon in 2016 and 2021. The RF method was then used to generate water extraction results.

Table 9 | District-wise change in surface water area (km^2) during pre- and post-monsoon 2021

Sl.	District	Non-water bodies	Water gain	Water loss	Water bodies
1	Bishnupur	415.80	23.71	16.76	104.67
2	Chandel	2,477.72	0.57	0.76	3.55
3	Churachandpur	3,499.34	3.13	1.11	8.83
4	Imphal East	389.09	0.79	0.99	1.75
5	Imphal West	342.48	18.08	25.72	56.31
6	Jiribam	172.04	0.23	0.28	1.66
7	Kakching	203.09	13.40	30.38	10.71
8	Kamjong	1,673.40	0.21	0.30	1.21
9	Kangpokpi	800.60	0.59	0.74	7.63
10	Noney	1,507.02	2.00	2.05	9.07
11	Pherzwal	1,118.48	0.71	0.91	6.05
12	Senapati	2,788.57	0.74	0.99	1.84
13	Tamenglong	2,642.67	1.42	1.74	5.54
14	Tengnoupal	841.41	0.11	0.12	0.05
15	Thoubal	308.96	7.09	18.74	22.47
16	Ukhrul	2,820.73	1.03	1.87	2.20

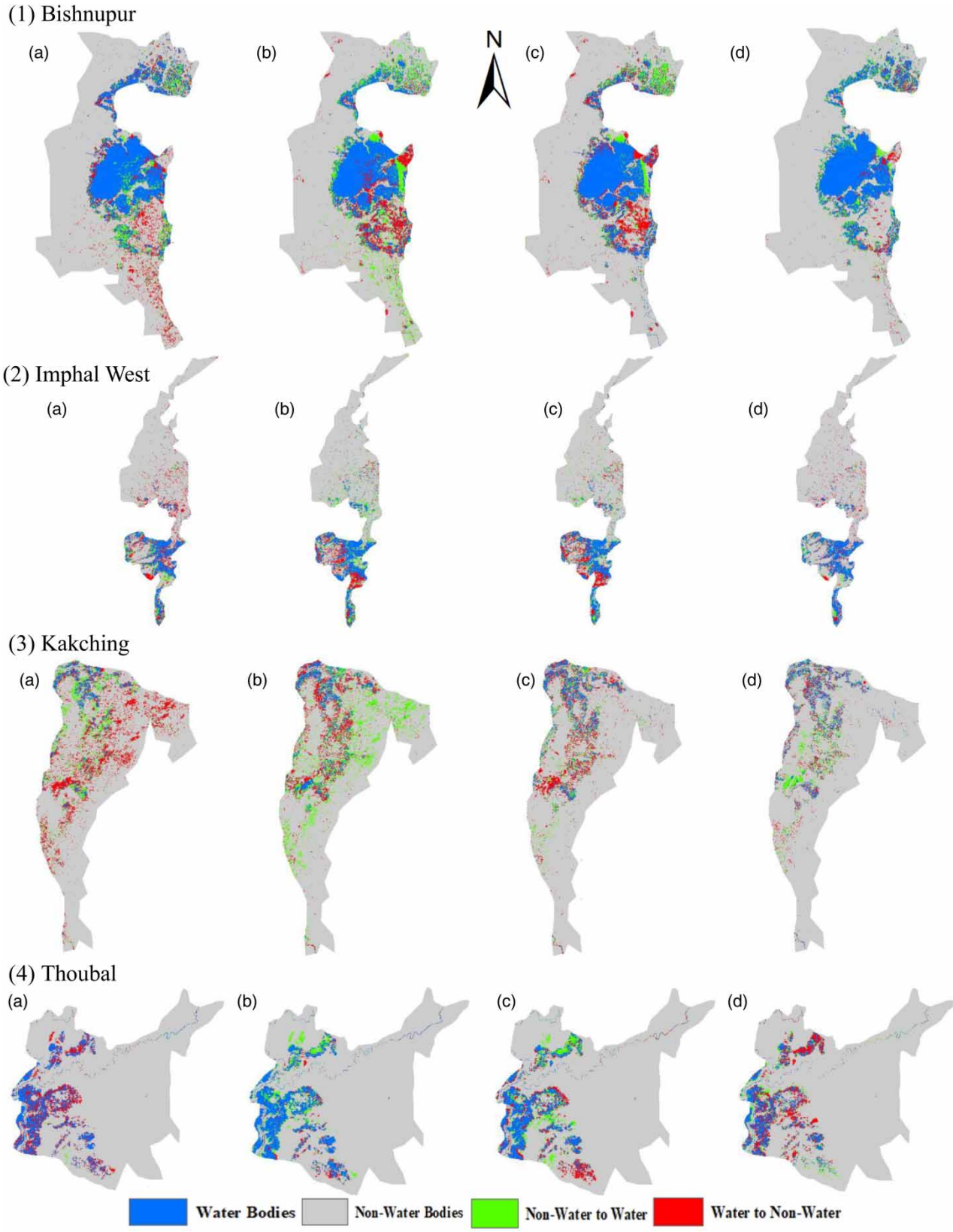

Figure 7 | Significant surface water spread change at different districts of Manipur during (a) PoM 2016 to PoM 2021, (b) PrM 2016 to PoM 2016, (c) PrM 2016 to PrM 2021, and (d) PrM 2021 to PoM 2021 at (1) Bishnupur, (2) Imphal West, (3) Kakching, and (4) Thoubal.

Verifications were done from Joint Research Centre datasets from 16 March 1984 and 31 December 2020 that are freely available in the GEE platform to check the proposed effectiveness of the framework. The proposed method has overall accuracy and a relatively high kappa coefficient. Meanwhile, related to the state-of-the-art method, the Otsu threshold approach in terms of qualitative and quantitative evaluations, the proposed water extraction framework employing the RF method can provide better performance. Argenti *et al.* (2013) emphasized the challenges of setting initial and automated thresholds. Speedy and less computationally intensive threshold segmentation methods pose difficulty due to dependence on various parameters such as wavelength, incidence angle, and dielectric characteristics.

Mapping surface water with Sentinel-2 in the GEE platform encountered issues with clouds and shadows, particularly in high-altitude regions. Cloud masking algorithms proved effective against clouds while removing mountain shadows using the AWEI-sh Index, and Digital Elevation Model (DEM) enhanced water continuity. However, selecting optimal textural elements for water extraction remained challenging, and mitigating shadow effects was complex. Overcoming water continuity issues in large-scale imagery was crucial. Zhang *et al.* (2018) highlighted the GEE platform's role in improving efficiency for large-scale and time series surface water dynamics studies. They proposed using level-set segmentation with Sentinel-1 data, reducing shadow and noise interference, leading to enhanced accuracy in water feature extraction, particularly in hilly regions.

About 90% of Manipur is hilly regions, so mountain shadows were challenging to remove directly from water extraction findings. Therefore, the DEM was utilized to construct a slope model, which was beneficial in eliminating mountain shadows. After initial water extraction calculations, the mean slope was computed, and the shadows were eliminated for slopes exceeding 15 degrees, as described by Li & Sheng (2012) and Jiang *et al.* (2021). Moreover, merging the open and closed procedures of the mathematical morphology model enhances the accuracy of small water bodies.

The analysis has identified a concerning trend in most districts of Manipur where water bodies are consistently shrinking (potential droughts in the study area for 2019 and 2021), whether during the pre-monsoon or monsoon periods from 2016 to 2021. This ongoing reduction in water bodies contributes to water stress scenarios across Manipur. Consequently, there is an urgent need for enhanced water resource management to promote sustainable development and preserve the regional ecological balance.

5. CONCLUSIONS

This study employs advanced remote sensing techniques to analyze surface water dynamics in Manipur, providing crucial insights into water resources management, sustainable development, and environmental conservation. By harnessing technologies such as GEE and Sentinel-2 datasets, the research sets a precedent for integrating technological solutions into regional resource management, enhancing accuracy and efficiency.

In water resources planning, the study delivers a high-resolution mapping of surface water dynamics in Manipur, offering vital insights into water availability and distribution. Identifying diminishing water bodies underscores the impact of climate change, emphasizing the necessity for adaptive strategies to mitigate water stress. Key findings include determining maximum and minimum surface water areas in various districts during pre-monsoon and post-monsoon periods, facilitating more efficient resource allocation by decision-makers. The observed decline in water bodies poses a direct threat, emphasizing the urgency of enhanced water resource management for sustainable use and regional well-being. Significantly, the negligible water loss in the Churachandpur district indicates a stable water ecosystem, guiding conservation efforts. The effectiveness of the RF classifier method in surface water extraction holds practical implications for land use and development decisions, fostering sustainability.

Recognizing the concerning trend of diminishing water bodies underscores the need for proactive measures to uphold ecosystem health and biodiversity. The study's results extend beyond scientific inquiry, providing tangible implications for addressing water challenges in Manipur. This information can inform policies, empower communities, and guide regional efforts towards a sustainable and resilient future.

Based on the study, the main conclusions are listed as follows:

(1) Among the selected districts of Manipur, the maximum surface water area found at Bishnupur is 123.62 km^2, and the minimum surface water area was observed at Tengnoupal as 0.24 km^2 during pre-monsoon for the study period from 2016 to 2021.

(2) For post-monsoon from 2016 to 2021, the maximum surface water area of 100.03 km^2 was observed at Bishnupur, whereas a minimum surface water area of 0.21 km^2 for Pherzwal district.
(3) The findings of the change analysis revealed that the maximum water gain was 6% in the Bishnupur district during pre- and post-monsoon for the year 2016, and the minimum water gain was 9.5×10^{-3}% in the Tengnoupal district for post-monsoon during 2016 and 2021.
(4) The findings of the change analysis revealed that the maximum water loss was 7% in the Bishnupur district for pre-monsoon during 2016 and 2021.
(5) Almost negligible water loss was found in the Churachandpur district during pre- and post-monsoon for 2016.
(6) Compared to the Otsu thresholding method, the RF classifier method is profoundly satisfactory for surface water extraction.

DATA AVAILABILITY STATEMENT

Data cannot be made publicly available; readers should contact the corresponding author for details.

CONFLICT OF INTEREST

The authors declare there is no conflict.

REFERENCES

Acharya, T. D., Lee, D. H., Yang, I. T. & Lee, J. K. 2016 Identification of water bodies in a Landsat 8 OLI image using a J48 decision tree. *Sensors* **16** (7), 1075.

Allen, G. H. & Pavelsky, T. M. 2015 Patterns of river width and surface area revealed by the satellite-derived North American River Width data set. *Geophysical Research Letters* **42** (2), 395–402.

Argenti, F., Lapini, A., Bianchi, T. & Alparone, L. 2013 A tutorial on speckle reduction in synthetic aperture radar images. *IEEE Geoscience and Remote Sensing Magazine* **1** (3), 6–35.

Atay, M. A. & Kaplan, G. 2023 Large-scale mapping of inland waters with Google Earth Engine using remote sensing. *Environmental Sciences Proceedings* **25** (1), 52.

Balázs, B., Bíró, T., Dyke, G., Singh, S. K. & Szabó, S. 2018 Extracting water-related features using reflectance data and principal component analysis of Landsat images. *Hydrological Sciences Journal* **63** (2), 269–284.

Chen, Z. & Zhao, S. 2022 Automatic monitoring of surface water dynamics using Sentinel-1 and Sentinel-2 data with Google Earth Engine. *International Journal of Applied Earth Observation and Geoinformation* **113**, 103010.

Chen, C., Qin, Q., Zhang, N., Li, J., Chen, L., Wang, J., Qin, X. & Yang, X. 2014 Extraction of bridges over water from high-resolution optical remote-sensing images based on mathematical morphology. *International Journal of Remote Sensing* **35** (10), 3664–3682.

Crist, E. P. 1985 A TM tasseled cap equivalent transformation for reflectance factor data. *Remote Sensing of Environment* **17** (3), 301–306.

Dehkordi, A. T., Valadan Zoej, M. J., Ghasemi, H., Jafari, M. & Mehran, A. 2022 Monitoring long-term spatiotemporal changes in Iran surface waters using landsat imagery. *Remote Sensing* **14** (18), 4491.

Deng, Z., Sun, Y., Zhang, K., Qiu, Q. & Sun, W. 2020 A water identification method basing on grayscale Landsat 8 OLI images. *Geocarto International* **35** (7), 700–710.

Feng, M., Sexton, J. O., Channan, S. & Townshend, J. R. 2016 A global, high-resolution (30-m) inland water body dataset for 2000: First results of a topographic–spectral classification algorithm. *International Journal of Digital Earth* **9** (2), 113–133.

Feyisa, G. L., Meilby, H., Fensholt, R. & Proud, S. R. 2014 Automated water extraction index: A new technique for surface water mapping using Landsat imagery. *Remote Sensing of Environment* **140**, 23–35.

Fisher, A., Flood, N. & Danaher, T. 2016 Comparing Landsat water index methods for automated water classification in eastern Australia. *Remote Sensing of Environment* **175**, 167–182.

Frazier, P. S. & Page, K. J. 2000 Water body detection and delineation with Landsat TM data. *Photogrammetric Engineering and Remote Sensing* **66** (12), 1461–1467.

Giardino, C., Bresciani, M., Villa, P. & Martinelli, A. 2010 Application of remote sensing in water resource management: The case study of lake Trasimeno, Italy. *Water Resources Management* **24** (14), 3885–3899.

Goffi, A., Stroppiana, D., Brivio, P. A., Bordogna, G. & Boschetti, M. 2020 Towards an automated approach to map flooded areas from Sentinel-2 MSI data and soft integration of water spectral features. *International Journal of Applied Earth Observation and Geoinformation* **84**, 101951.

Gorelick, N., Hancher, M., Dixon, M., Ilyushchenko, S., Thau, D. & Moore, R. 2017 Google earth engine: Planetary-scale geospatial analysis for everyone. *Remote Sensing of Environment* **202**, 18–27.

Halder, B., Barman, S., Banik, P., Das, P., Bandyopadhyay, J., Tangang, F., Shahid, S., Pande, C. B., Al-Ramadan, B. & Yaseen, Z. M. 2023 Large-scale flood hazard monitoring and impact assessment on landscape: representative case study in India. *Sustainability* **15** (14), 11413.

Horkaew, P. & Puttinaovarat, S. 2017 Entropy-Based fusion of water indices and DSM derivatives for automatic water surfaces extraction and flood monitoring. *ISPRS International Journal of Geo-Information* **6** (10), 301.

Huang, C., Chen, Y., Zhang, S. & Wu, J. 2018 Detecting, extracting, and monitoring surface water from space using optical sensors: A review. *Reviews of Geophysics* **56** (2), 333–360.

Ji, L., Zhang, L. & Wylie, B. 2009 Analysis of dynamic thresholds for the normalized difference water index. *Photogrammetric Engineering & Remote Sensing* **75** (11), 1307–1317.

Jiang, H., Wang, M., Hongda, H. & Jianhui, X. 2021 Evaluating the performance of Sentinel-1a and Sentinel-2 in small waterbody mapping over urban and mountainous regions. *Water (Switzerland)* **13** (7), 945.

Jiang, L., Zhou, C. & Li, X. 2023 Sub-pixel surface water mapping for heterogeneous areas from Sentinel-2 images: A case study in the Jinshui Basin, China. *Water* **15** (8), 1446.

Kandekar, V. U., Pande, C. B., Rajesh, J., Atre, A. A., Gorantiwar, S. D., Kadam, S. A. & Gavit, B. 2021 Surface water dynamics analysis based on sentinel imagery and Google Earth Engine Platform: A case study of Jayakwadi dam. *Sustainable Water Resources Management* **7** (3), 44.

Kaplan, G. & Avdan, U. 2017 Object-based water body extraction model using Sentinel-2 satellite imagery. *European Journal of Remote Sensing* **50** (1), 137–143.

Karpatne, A., Khandelwal, A., Chen, X., Mithal, V., Faghmous, J. & Kumar, V. 2016 Global monitoring of inland water dynamics: State-of-the-art, challenges, and opportunities. *Computational Sustainability* **645**, 121–147.

Klein, I., Dietz, A., Gessner, U., Dech, S. & Kuenzer, C. 2015 Results of the global waterpack: A novel product to assess inland water body dynamics on a daily basis. *Remote Sensing Letters* **6** (1), 78–87.

Lake, P. S. 2003 Ecological effects of perturbation by drought in flowing waters. *Freshwater Biology* **48** (7), 1161–1172.

Laonamsai, J., Julphunthong, P., Saprathet, T., Kimmany, B., Ganchanasuragit, T., Chomcheawchan, P. & Tomun, N. 2023 Utilizing NDWI, MNDWI, SAVI, WRI, and AWEI for estimating erosion and deposition in ping river in Thailand. *Hydrology* **10** (3), 70.

Lepcha, P. T., Pandey, P. K. & Ranjan, P. 2021 Hydrological significance of Himalayan surface water and its management considering anthropogenic and climate change aspects. *IOP Conference Series: Materials Science and Engineering* **1020** (1), 012013.

Lepcha, P. T., Pandey, P. K. & Pandey, V. 2024 Quantification of the impact of land cover and climate change on water and sediment yield in sub-tropical Himalayas in upstream Teesta river basin. *Sikkim. Remote Sensing Applications: Society and Environment* **34**, 101146.

Li, J. & Sheng, Y. 2012 An automated scheme for glacial lake dynamics mapping using Landsat imagery and digital elevation models: A case study in the Himalayas. *International Journal of Remote Sensing* **33** (16), 5194–5213.

Li, C., Xue, D., Zhang, L. & Su, L. 2018 Research on water extraction method based on Sentinel-1A satellite SAR data. *Geo-spatial Information* **16**, 37–40.

Li, J., Peng, B., Wei, Y. & Ye, H. 2021a Accurate extraction of surface water in complex environment based on Google Earth Engine and Sentinel-2. *PLoS ONE* **16** (6), e0253209.

Li, X., Ling, F., Foody, G. M., Boyd, D. S., Jiang, L., Zhang, Y., Zhou, P., Wang, Y., Chen, R. & Du, Y. 2021b Monitoring high spatiotemporal water dynamics by fusing MODIS, Landsat, water occurrence data and DEM. *Remote Sensing of Environment* **265**, 112680.

Li, J., Ma, R., Cao, Z., Xue, K., Xiong, J., Hu, M. & Feng, X. 2022 Satellite detection of surface water extent: A review of methodology. *Water* **14** (7), 1148.

Liao, A., Chen, L., Chen, J., He, C., Cao, X., Chen, J., Peng, S., Sun, F. & Gong, P. 2014 High-resolution remote sensing mapping of global land water. *Science China Earth Sciences* **57** (10), 2305–2316.

Liu, X., Zhang, J., Ma, D., Bao, Y., Tong, Z. & Liu, X. 2013 Dynamic risk assessment of drought disaster for maize based on integrating multi-sources data in the region of the northwest of Liaoning Province, China. *Natural Hazards* **65** (3), 1393–1409.

Mayer, T., Poortinga, A., Bhandari, B., Nicolau, A. P., Markert, K., Thwal, N. S., Markert, A., Haag, A., Kilbride, J., Chishtie, F., Wadhwa, A., Clinton, N. & Saah, D. 2021 Deep learning approach for Sentinel-1 surface water mapping leveraging Google Earth Engine. *ISPRS Open Journal of Photogrammetry and Remote Sensing* **2**, 100005.

McFeeters, S. K. 1996 The use of the normalized difference water index (NDWI) in the delineation of open water features. *International Journal of Remote Sensing* **17** (7), 1425–1432.

Mohammadi, A., Costelloe, J. F. & Ryu, D. 2017 Application of time series of remotely sensed normalized difference water, vegetation and moisture indices in characterizing flood dynamics of large-scale arid zone floodplains. *Remote Sensing of Environment* **190**, 70–82.

Nguyen, T. T., Nguyen, T. T., Phan, C. T. & Nguyen, Q. V. H. 2022 A unified framework for water surface extraction and change prediction in imagery data streams. *Journal of Computer Science and Cybernetics* **38** (1), 85–102.

Nyatuame, M., Amekudzi, L. K. & Agodzo, S. K. 2020 Assessing the land use/land cover and climate change impact on water balance on Tordzie watershed. *Remote Sensing Applications: Society and Environment* **20**, 100381.

Olthof, I. 2017 Mapping seasonal inundation frequency (1985–2016) along the St-John River, New Brunswick, Canada using the landsat archive. *Remote Sensing* **9** (2), 143.

Ozesmi, S. L. & Bauer, M. E. 2002 Satellite remote sensing of wetlands. *Wetlands Ecology and Management* **10**, 381–402.

Palmer, S. C. J., Kutser, T. & Hunter, P. D. 2015 Remote sensing of inland waters: Challenges, progress and future directions. *Remote Sensing of Environment* **157**, 1–8.

Papa, F., Crétaux, J. F., Grippa, M., Robert, E., Trigg, M., Tshimanga, R. M., Kitambo, B., Paris, A., Carr, A., Fleischmann, A. S., de Fleury, M., Gbetkom, P. G., Calmettes, B. & Calmant, S. 2023 Water resources in Africa under global change: monitoring surface waters from space. *Surveys in Geophysics* **44** (1), 43–93.

Park, Y., Pyo, J., Kwon, Y. S., Cha, Y., Lee, H., Kang, T. & Cho, K. H. 2017 Evaluating physico-chemical influences on cyanobacterial blooms using hyperspectral images in inland water, Korea. *Water Research* **126**, 319–328.

Rapinel, S., Mony, C., Lecoq, L., Clément, B., Thomas, A. & Hubert-Moy, L. 2019 Evaluation of Sentinel-2 time-series for mapping floodplain grassland plant communities. *Remote Sensing of Environment* **223**, 115–129.

Richter, R., Louis, J. & Berthelot, B. 2012 Sentinel-2 MSI – level 2A products algorithm theoretical basis document. *European Space Agency, (Special Publication) ESA SP* **49** (0), 1–72.

Rokni, K., Ahmad, A., Solaimani, K. & Hazini, S. 2016 A new approach for detection of surface water changes based on principal component analysis of multitemporal normalized difference water index. *Journal of Coastal Research* **32** (2), 443.

Saghafi, M., Ahmadi, A. & Bigdeli, B. 2021 Sentinel-1 and Sentinel-2 data fusion system for surface water extraction. *Journal of Applied Remote Sensing* **15** (1), 014521–014521.

Singh, A. M. 2022 Flood mapping in valley districts of manipur using satellite-based synthetic aperture radar (SAR) images. *Ecology Environment and Conservation* **28**, S481–S488.

Singh, K. V., Setia, R., Sahoo, S., Prasad, A. & Pateriya, B. 2015 Evaluation of NDWI and MNDWI for assessment of waterlogging by integrating digital elevation model and groundwater level. *Geocarto International* **30** (6), 650–661.

Sogno, P., Klein, I. & Kuenzer, C. 2022 Remote sensing of surface water dynamics in the context of global change – A review. *Remote Sensing* **14** (10), 2475.

Sur, K., Verma, V. K. & Pateriya, B. 2021 Surface water estimation at regional scale using hybrid techniques in GEE environment – A case study on Punjab State of India. *Remote Sensing Applications: Society and Environment* **24**, 100625.

Teklu, B. M., Adriaanse, P. I., Ter Horst, M. M. S., Deneer, J. W. & Van den Brink, P. J. 2015 Surface water risk assessment of pesticides in Ethiopia. *Science of the Total Environment* **508**, 566–574.

Tralli, D. M., Blom, R. G., Zlotnicki, V., Donnellan, A. & Evans, D. L. 2005 Satellite remote sensing of earthquake, volcano, flood, landslide and coastal inundation hazards. *ISPRS Journal of Photogrammetry and Remote Sensing* **59** (4), 185–198.

Tran, K. H., Menenti, M. & Jia, L. 2022 Surface water mapping and flood monitoring in the Mekong delta using Sentinel-1 SAR time series and otsu threshold. *Remote Sensing* **14** (22), 5721.

Vörösmarty, C. J., Green, P., Salisbury, J. & Lammers, R. B. 2000 Global water resources: Vulnerability from climate change and population growth. *Science* **289** (5477), 284–288.

Wang, H., Liu, X., Wang, Y., Zhang, S., Zhang, G., Han, Y., Li, M. & Liu, L. 2023 Spatial and temporal dynamics of microbial community composition and factors influencing the surface water and sediments of urban rivers. *Journal of Environmental Sciences* **124**, 187–197.

Xie, H., Luo, X., Xu, X., Pan, H. & Tong, X. 2016a Evaluation of Landsat 8 OLI imagery for unsupervised inland water extraction. *International Journal of Remote Sensing* **37** (8), 1826–1844.

Xie, H., Luo, X., Xu, X., Pan, H. & Tong, X. 2016b Automated subpixel surface water mapping from heterogeneous urban environments using Landsat 8 OLI imagery. *Remote Sensing* **8** (7), 584.

Xu, H. 2006 Modification of normalized difference water index (NDWI) to enhance open water features in remotely sensed imagery. *International Journal of Remote Sensing* **27** (14), 3025–3033.

Yan, Z. & Jinwei, D. 2019 Remote sensing of land surface water monitoring research progress. *Journal of Geo-Information Science* **21**, 1768–1778.

Yang, X., Zhao, S., Qin, X., Zhao, N. & Liang, L. 2017 Mapping of urban surface water bodies from Sentinel-2 MSI imagery at 10 m resolution via NDWI-based image sharpening. *Remote Sensing* **9** (6), 596.

Yang, X., Li, Y., Wei, Y., Chen, Z. & Xie, P. 2020 Water body extraction from Sentinel-3 image with multiscale spatiotemporal super-resolution mapping. *Water* **12** (9), 2605.

Zhang, K., Shi, H., Peng, J., Wang, Y., Xiong, X., Wu, C. & Lam, P. K. S. 2018 Microplastic pollution in China's inland water systems: A review of findings, methods, characteristics, effects, and management. *Science of the Total Environment* **630**, 1641–1653.

Zhu, J., Guo, H., Fan, X., Ding, C., Ligang, L. & Yulong, L. 2006 High-resolution SAR image water detection based on texture and imaging knowledge. *Advances in Water Science* **17**, 525–530.

First received 4 October 2023; accepted in revised form 16 February 2024. Available online 27 February 2024